revision 1

Balestraite, $KLi_2VSi_4O_{10}O_2$, the first member of the mica group with octahedral V^{5+}

G.O. LEPORE[1], L. BINDI[1], A. ZANETTI[2], M.E. CIRIOTTI[3], O. MEDENBACH[4], P. BONAZZI[1,*]

[1]Dipartimento di Scienze della Terra, Università di Firenze, Via La Pira 4, I-50121 Firenze, Italy

[2]Istituto di Geoscienze e Georisorse, CNR, UOS di Pavia, Via Ferrata 1, I-27100 Pavia, Italy

[3]Associazione Micromineralogica Italiana, via San Pietro 55, I-10073 Devesi-Ciriè, Italy

[4]Institut für Geologie, Mineralogie und Geophysik, Ruhr-Universität Bochum, D-44780 Bochum, Germany

*paola.bonazzi@unifi.it

ABSTRACT

A mica-group mineral characterized by a high V content and free of Al was found in the manganesiferous beds within the metacherts of the ophiolitic sequences at the Cerchiara mine, Eastern Liguria (Italy), in association with hematite, quartz and calcite. Chemical and structural characterization supported by Raman data defines this phase as a new mineral species, which is named balestraite after Corrado Balestra, a prominent Italian amateur mineralogist. Balestraite, ideally $KLi_2V^{5+}Si_4O_{10}O_2$, is a 1*M* trioctahedral mica crystallizing in the *C*2 space group, with a = 5.2024(5) Å, b = 8.9782(7) Å, c = 9.997(2) Å, β = 100.40(2)°, V = 459.3(1) Å^3, Z = 2. The reduction of symmetry from the "ideal" space group *C*2/*m* is related to the ordering of V at only one of the two pseudo-symmetric octahedral sites. Vanadium forms very distorted octahedra with a [2+2+2] geometry characteristic of the valence state +5. The Li,V composition of the octahedral sheet, the pure tetrasilicic character of the tetrahedral sheet, and the anhydrous character produce unusual geometrical features for this mica. The occurrence of 5+ as the dominant valence state of V and the virtually complete $O^{2-} \rightarrow OH^-$ substitution at the O4 site indicate strongly oxidizing conditions of crystallization, which are consistent with balestraite occurring at the

boundary between carbonate-bearing veins and hematite bands.

The new mineral and name were approved by the Commission on New Minerals, Nomenclature and Classification, IMA (2013-080).

Keywords: balestraite, new mineral, Li-mica, V-mica, Cerchiara mine, pentavalent vanadium

INTRODUCTION

Preliminary chemical analyses of a micaceous mineral found in the manganesiferous beds within the metacherts of the ophiolitic sequences at the Cerchiara mine, Eastern Liguria (Italy), showed a composition suggesting a new member of the mica group. In particular, data obtained via energy dispersive spectrometry (EDS) analyses on a polished section indicated an unusually high V content, and no other transition metals or Al. Muscovite and phlogopite with high V contents have been occasionally reported [e.g. Pan and Fleet (1992), Ankinovich et al. (2001) and Giuliani et al. (2008)]. Until now, however, the only known V-members of the mica group were roscoelite, ideally $KV_2[AlSi_3O_{10}(OH)_2]$ (Brigatti et al. 2003) and chernykhite, ideally $BaV_2[Al_2Si_2O_{10}(OH)_2]$ (Ankinovich et al. 1973). Thus, owing to the absence of Al, this mineral was worthy of further investigations.

The present paper reports the results of chemical, structural and spectroscopic studies to define and describe this new mica, which was named balestraite after Corrado Balestra (b. 1962), a prominent Italian amateur mineralogist and an expert of Ligurian minerals. The mineral and its name have been approved by the Commission on New Minerals, Nomenclature and Classification, IMA (2013-080). The holotype material is deposited in the mineralogical collections of the Museo di Storia Naturale, Università di Firenze (Italy), under catalogue number 3133/I.

GEOLOGICAL SETTING, OCCURRENCE AND PARAGENESIS

Balestraite was found in the ore body of the Cerchiara mine (~44°11'58"N, 9°42'1"E), which belongs to the well-known Mn district of Eastern Liguria named “Gambatesa district”. The ore body is located near the base of chert sequences (“Diaspri di Monte Alpe”

Formation) overlaying Jurassic ophiolites (Cortesogno et al. 1979; Lucchetti et al. 1988). The ore consists of rhythmic interlaying of braunite-bearing metasediments (5-15 cm thick) and hematite-rich cherts. According to Cabella et al. (1998), the primary Mn-oxide and hematite-rich cherts formed by fractionation from hydrothermally derived metalliferous siliceous muds during turbiditic re-sedimentation; subsequently, the sedimentary-diagenetic deposits were re-equilibrated under prehnite-pumpellyite facies conditions leading to a braunite + quartz stable assemblage. During this stage, reactions triggered by mobilized fluids along fractures produced Mn-silicate and Mn-carbonate assemblages at the expense of braunite + quartz. Successive decompressional tectonic evolution under decreasing *P-T* metamorphic conditions induced further concentration of dispersed elements, such as Ba, Sr, As, and V, to allow the genesis of a great variety of new and rare minerals in later extensional fractures. The carbonate veins exhibit boundaries which are locally enriched in alkaline and alkaline-earth elements, such as Li, Na and Ba (Cabella et al. 1990). Sugilite (Cabella et al. 1990), together with other unusual Li-rich phases such as norrishite and nambulite and small amounts of vanadiferous species like gamagarite, tokyoite and pyrobelonite, have been found (unpublished data).

Balestraite was found at the boundary between carbonate-bearing veins and hematite bands. The mineral forms a layered cluster, about 2 × 1 cm in size, of randomly packed crystals in contact with quartz and calcite (Fig. 1).

PHYSICAL AND OPTICAL PROPERTIES

Balestraite exhibits a tabular morphology, and does not show any inclusions of, or intergrowths with, other minerals. The maximum grain size of balestraite is about 400 μm. The mineral is pale yellow in color, transparent with silky lustre and does not fluoresce under short- and long-wave ultraviolet light. It is brittle (Mohs hardness between 2½ and 3) with uneven fracture and shows a perfect {001} cleavage. The calculated density is 2.946 g cm^{-3}, based on the empirical formula and the unit-cell dimensions determined by single-crystal X-ray diffraction (see below).

Balestraite is biaxial, optically negative with $\alpha = 1.642(2)$, $\beta = 1.664(2)$ and $\gamma = 1.676(2)$; the measured $2V$ is 84.4(2)° ($2V_{calc} = 72°$), and it has a distinct dispersion ($r < v$).

The mineral does not show pleochroism and its color is pale grey in thin section. Optical properties were measured using monochromatic Na light (λ = 589 nm) at room temperature.

EXPERIMENTAL METHODS

X-ray diffraction and structure refinement

Several platy crystals with variable lateral dimensions and thickness (volumes ranging from 1 to 400 $\cdot 10^4$ μm^3, approximately) were mounted on a 8 μm-diameter carbon fiber and examined on a CCD-equipped Oxford Diffraction Excalibur 3 diffractometer to avoid twinned and/or deformed crystals. In general, crystal quality was poor, with weak and very broad reflections, usually not sufficient even for unit-cell determination. After dozens of trials, a crystal (30 × 220 × 250 μm) suitable for full data collection, although far from optimal, was found. The refined unit-cell dimensions are: a = 5.2024(5), b = 8.9782(7), c = 9.997(2) Å, β = 100.40(2)° and V = 459.3(1) $Å^3$, suggesting that the mineral is a 1M polytype. Intensity integration and standard Lorentz-polarization corrections were performed with the *CrysAlis* RED software package (Oxford Diffraction 2006). The program ABSPACK in *CrysAlis* RED (Oxford Diffraction 2006) was used for the absorption correction, and the structure refinement was performed using the full matrix least-squares program SHELXL-97 (Sheldrick 2008). Initial attempts to refine the structure in the ideal space group $C2/m$ did not produce convergence. Ordering of the octahedral cations was considered with a decrease of symmetry to the $C2$ space group, starting from atomic coordinates given by Brigatti et al. (2000) for polylithionite. The refinement in this subgroup led to an improvement of the R factor (with R_1 decreasing from 0.261 to 0.223 for the isotropic model), without significant correlation between parameters of the pseudo-mirror related atoms. Attempts to refine a Cm model, which produces disorder of the octahedral cations, led to higher R factor (R_1 = 0.240 for the isotropic model) with an unreliable isotropic thermal parameter for O4.

Scattering curves for ionized Li, O, Si, and V as well as $\Delta f'$, $\Delta f''$ coefficients were taken from Wilson and Prince (1999). The site occupancy factors were initially allowed to vary (Li^+ vs. V^{5+}) for the three independent M sites; M1 was found to be fully occupied by Li and fixed accordingly. Refinement of the anisotropic atomic displacement parameters

was possible only for T1, T2 and M2 (nearly totally occupied by V), whereas for M1 and M3 (nearly totally occupied by Li) and the oxygen atoms an isotropic model was maintained. The final R_1 indices of 0.127 [for 1302 reflections with $F_o > 4\sigma(F_o)$] and 0.138 (for all 1587 independent reflections) were considered acceptable given the quality of the crystal. The refined Flack parameter (Parsons and Flack 2004) of 0.08(2) is consistent with a highly asymmetrical distribution of the enantiomorphic components and indicates that the acentric model is correct. Details of the data collection and refinement are given in Table 1, final atomic coordinates and isotropic displacement parameters are listed in Table 2, and anisotropic displacement parameters are in Table 3. Table 4[1] lists the observed and calculated structure factors.

The diffraction rings from few grains of balestraite were collected with a CCD-equipped diffractometer Xcalibur PX Ultra using Cu*K*α radiation (50 kV and 40 mA) and then converted into a conventional XRD pattern. The crystal-to-detector distance was 7 cm. Data were processed using the *CrysAlis* software package version 1.171.31.2 (Oxford diffraction 2006) running on the Xcalibur PX control PC. Observed and calculated X-ray powder diffraction data are listed in Table 5. The unit-cell parameters from powder data are: $a = 5.2087(2)$, $b = 8.9991(3)$, $c = 10.0304(4)$ Å, $\beta = 100.354(3)°$ and $V = 462.51(2)$ Å^3, in fair agreement with the values obtained from single-crystal data (Table 1).

Chemical analyses

A crystal of about 450 × 180 × 50 μm was embedded in epoxy and polished for electron microprobe analysis, which was obtained with a JEOL 8200 electron microprobe at the Dipartimento di Scienze della Terra of the University of Milan (Italy) in wavelength dispersion mode at 15 kV, 5 nA beam current, and 10 μm as the beam size. The following standards were used: wollastonite (Si*K*α), K-feldspar (K*K*α), pure vanadium (V*K*α), and rhodonite (MnKα). Five point analyses on different spots were performed. Na, Mg, Ca, Ba, Al, Ti, F, and Cl were below 0.01 wt%. The crystal fragment was found to be homogeneous within analytical uncertainty.

[1] For a copy of Table 4, document item AMxxxxx, contact the Business Office of the Mineralogical Society of America (see inside front cover of recent issue) for price information. Deposit items may also be available on the American Mineralogist web site at http://www.minsocam.org.

In situ analysis of the content of Li was performed using laser-ablation inductively-coupled-plasma mass-spectrometry (LA-ICP-MS). The laser probe consists of a Q-switched Nd:YAG laser, model Quantel (Brilliant), whose fundamental emission in the near-IR region (1064 nm) was converted into 266 nm wavelength using two harmonic generators. Spot diameter was near 40-50 μm. The ablated material was analyzed by using an Elan DRC-e quadrupole mass spectrometer. Helium was used as the carrier gas and mixed with Ar downstream of the ablation cell. Data reduction was performed using the Glitter Software. NIST SRM 610 was analyzed as an external standard, whereas the SiO_2 was used as an internal standard. Precision and accuracy were assessed from repeated analyses of the BCR-2g, NIST SRM 612 and 610 standards and resulted in better than ± 3%. Full analytical details are reported in Tiepolo et al. (2005) and Miller et al. (2007).

Table 6 reports the chemical analyses (means and ranges in wt% of oxides), standard deviations and atomic ratios calculated on 12 oxygen atoms per formula unit (*pfu*) assuming balestraite as completely anhydrous and all vanadium at the pentavalent state, as indicated by the spectroscopic and structural analysis, respectively (see below).

Raman Spectroscopy

A Raman spectrum was obtained using a micro/macro Jobin Yvon LabRam HRVIS, equipped with a motorized x-y stage and an Olympus microscope. The backscattered Raman signal was collected with 50× objective and the Raman spectrum was obtained for a randomly oriented crystal. The 632.8 nm line of an He-Ne laser was used as excitation; laser power was controlled by a series of density filters. The lateral and depth resolution were about 2 and 5 μm, respectively. The system was calibrated using the 520.6 cm^{-1} Raman band of silicon before the experimental session. Spectra were collected with multiple acquisitions (2 to 6) with single counting times ranging between 20 and 180 seconds. The spectrum was recorded using the LabSpec 5 program from 150 to 4000 cm^{-1}.

Electron Paramagnetic Resonance

The EPR measurement was carried out on a Bruker ER 200D-SRC spectrometer operating at X-Band (~9.5 GHz) interfaced with DS/EPR software to a PC for data acquisition and handling; the actual operating frequency value was determined by using DPPH radical [2,2-di(4-tert-octyl-phenyl)-1-picrylhydrazyl, g = 2.0037] as external

standard. The spectrum was registered inserting the crystal into an amorphous silica tube, at room temperature. Under the adopted operating conditions (100 KHz modulation frequency, 4 db modulation amplitude), the minimum amount of detectable V can be estimated in $5 \cdot 10^{13}$ ions (Burns and Flockhart 1990). This value corresponds to ~0.01% of the total V content in the sample, given the experimental volume (about $19 \cdot 10^{6}$ μm^3, approximately) and the density of the investigated sample.

RESULTS

The crystal structure of balestraite is topologically similar to that of the other trioctahedral micas belonging to the 1*M* polytype; however, the mineral is characterized by unusual geometrical features related to its Li,V - rich chemical composition. Consistent with many the Li-rich micas (e.g., Brigatti et al. 2007 and references therein), balestraite crystallizes in the *C*2 space group. The reduction of symmetry from the ideal space group *C*2/*m* is related to the ordering of V at one (M2) of the two *cis*-octahedral sites (M2 and M3), whereas Li almost fully occupies the other two sites (Table 2, Fig. 2). This ordering scheme is consistent with the site scattering (21.6 e^- in M2 vs. 3.0 and 3.6 in M1 and M3, respectively) and the geometry of the three octahedra.

The analysis of the Raman spectrum (Fig. 3) shows no peaks in the region of the O-H stretching band (3300-3800 cm^{-1}) thus suggesting balestraite to be anhydrous. In this light, charge balance would require all vanadium at the pentavalent state. This feature is indeed confirmed observing the geometry of the M2 polyhedron which exhibits a V-O bond-length distribution characteristic of the valence state +5 (Schindler et al. 2000), showing a [2+2+2] coordination with two short vanadyl bonds (1.66 Å) with O4 in a *cis* arrangement, two longer *equatorial* bonds (1.985 Å) with O32, and the two longest bonds (2.184 Å) with O31 *trans* to the vanadyl anions (Fig. 4). Furthermore, EPR spectrum shows no absorption signal due to V^{4+} (the only V species with odd number of unpaired electrons), thus allowing to exclude significant amounts of V^{4+} and making unlikely the presence of V^{3+}.

The octahedral V^{5+} is also supported by a high-wavenumber Raman band (973 cm^{-1}), consistent with what reported by Frost et al. (2005) for symmetric vibrational modes from $V^{5+}O_6$ units in decavanadate minerals, including pascoite (three bands at 991, 965, 958 cm^-

211 ^{1}) and hummerite (two bands at 999 - 962 cm^{-1}).

212 The empirical formula (based on V as V^{5+} and O4 occupied by O^{2-}) is
213 $K_{0.99}Li_{2.00}V^{5+}_{0.97}Si_{4.04}O_{12}$ and this result is consistent with the structure refinement and close
214 to the simplified formula of $KLi_2V^{5+}[Si_4O_{10}O_2]$. The electron count calculated on the basis
215 of the empirical formula for the octahedral sites (28.3) is in excellent accord with that
216 obtained by the structure refinements (28.2).
217
218 ## DISCUSSION
219 **Octahedral sheet**
220 <M1-O> and <M3-O> bond lengths (2.08 and 2.10 Å, respectively) are similar to
221 those found for Li-rich octahedra (e.g., Tyrna and Guggenheim 1991; Brigatti et al. 2000,
222 2007). M1 and M3 octahedra are flattened and less distorted in comparison with M2, which
223 is strongly influenced by the presence of V^{5+} (see Table 7 and 8 for details). The
224 trioctahedral sheet in balestraite is affected by the ordering of cations with markedly
225 different size and charge, whereas the "oxy" component only marginally affects the
226 octahedral bond lengths. Divalent anions (O^{2-}) at O4 would be expected to increase the
227 electrostatic attraction with all M cations, such as in "oxybiotite" (Ohta et al. 1982), thus
228 inducing a shortening of all the M-O4 distances. This feature, observed also in norrishite,
229 $KLiMn^{3+}_2[Si_4O_{10}O_2]$ (Tyrna and Guggenheim 1991), may be related to the presence of Li^+.
230 However, this trend occurs only for M2, whereas M1-O4 and M3-O4 are longer than the
231 others (Table 7). Thus a high and positive off-center shift value, usually indicating sensible
232 amounts of "oxy" component in trioctahedral *C*2/*m* micas (Cesare et al. 2003; Mesto et al.
233 2006; Gianfagna et al. 2007; Matarrese et al. 2008; Scordari et al. 2008, 2010), is only
234 observed for M2 (0.316 Å) whereas a negative value is shown by M3 (-0.198 Å).
235 Bond valence sums (BVS) for O1, O21, O22, O31 and O32 are all slightly higher
236 than 2.0 v.u. (Table 9), whereas the BVS for O4, despite the very short M2-O4 bonds, is
237 1.74 v.u.. A low value, however, does not require the presence of H, as documented for
238 other anhydrous or partially anhydrous members of the mica group (norrishite, BVS_{O4} =
239 1.69 v.u., Tyrna and Guggenheim 1991; oxykinoshitalite, BVS_{O4} = 1.54 v.u., Kogarko et al.
240 2005; oxyphlogopite, BVS_{O4} = 1.61 v.u., Chukanov et al. 2011).

241

242 **Tetrahedral sheet**

243 The tetrahedral sheet of balestraite is characterized by nearly perfect hexagonal rings;
244 the tetrahedral rotation angle α of 0.2° is the lowest value found in natural micas (Brigatti
245 and Guggenheim 2002). This feature is probably related to the small lateral dimensions of
246 the Si_4 tetrahedral sheet compared to the lateral dimensions of the octahedral sheet which,
247 owing to the Li,V composition, is one of the most contracted among the trioctahedral micas
248 leading to very short *a* and *b* cell edges.

249 Basal oxygen plane is corrugated in a similar manner to that observed in other Li-rich
250 micas (Brigatti and Guggenheim 2002 and references therein) with O1 and O21 atoms
251 drawn towards the octahedral sheet ($\Delta z = 0.087$).

252 Tetrahedra in balestraite are elongated parallel to $c\sin\beta$ with the mean pyramidal
253 edges length longer than the basal edges (2.670 vs. 2.591 Å for T1 and 2.671 vs. 2.603 Å
254 for T2). This difference in length reduces the basal surface and contributes to the decrease
255 of the lateral dimensions of the sheet. Tetrahedra in balestraite are distorted, as indicated by
256 the high values of BLD (bond length distortion) and τ (defined as the mean O_{basal}-T-O_{apical}
257 angle) parameters (Table 8). The high BLD values are related to the short T-O_{apical} distances:
258 whereas the mean Si-O bond lengths (1.61 and 1.62 Å for T1 and T2, respectively) are
259 close to the expected tetrahedral Si-O bond length of 1.623 Å on the basis of predictive
260 equation proposed by Baur (1978), the Si-O_{apical} are significantly shorter (1.560 and 1.586
261 Å for both T1 and T2, respectively). The displacement of Si towards the apical oxygens
262 may be related to high Si content. The high BVS on O1, O21 and O22 (Table 9) is not
263 capable of being directly balanced by any other substitutional mechanism. In contrast, for
264 the apical oxygen atoms, the presence of Si alone in the tetrahedra and V^{5+} in the adjacent
265 octahedron is balanced by the concomitant entry of a monovalent cation (Li).

266 The magnitude of the tetrahedral distortion, τ, is among the highest ever found in
267 natural micas (Brigatti and Guggenheim 2002): this observation, together with the
268 displacement of Si towards the apical oxygen atom, describes the elongated shape of the
269 tetrahedra. This feature is observed also in norrishite (Tyrna and Guggenheim 1991) and in
270 synthetic polylithionite, $KLi_2AlSi_4O_{10}F_2$ (Takeda and Burnham 1969) and, although to a

lesser extent, in tainiolite, $KLiMg_2Si_4O_{10}F_2$ (Toraya et al. 1977) and synthetic cesian tainiolites (Mariychuk et al. 2007; Baumgartner et al. 2009; Koch and Breu 2013).

Interlayer

The interlayer is occupied by very regular KO_{12} polyhedra with a short mean bond length of 3.066 Å. One of the most striking feature is the homogeneity of the K-O distances with <K-O_{inner}> matching <K-O_{outer}> (Table 8). This geometrical arrangement indicates nearly perfect hexagonal symmetry of the tetrahedral sheet and is also related to the small size of the tetrahedra. The interlayer thickness of only 3.26 Å, together with those observed in norrishite (3.27 Å; Tyrna and Guggenheim 1991) and oxykinoshitalite (3.221 Å; Kogarko et al. 2005), is among the lowest values found in trioctahedral micas (Brigatti and Guggenheim 2002) and contributes to the very short length of the *c* cell edge (9.997 Å). The small thickness is related to the absence of electrostatic repulsion usually occurring between the interlayer cation and the hydrogen bonded to O4 and here occupied by a divalent anion alone as first suggested by Cruciani and Zanazzi (1994) and then observed in hydrogen depleted micas of recent investigation (e.g. Schingaro et al. 2011; Scordari et al, 2013).

CONSTRAINTS ON PETROGENESIS

In terrestrial geological systems, vanadium exists as V^{3+}, V^{4+} and V^{5+}, with V^{5+} relative content increasing with oxygen activity (fO_2) (Canil 2002; Zanetti et al. 2004). The occurrence of 5+ as the dominant valence state of V in balestraite is thus consistent with strongly oxidizing conditions of crystallization, which are supported also by the complete $O^{2-} \rightarrow OH^-$ substitution at the O4 position and by the occurrence of balestraite at the boundary between carbonate-bearing veins and hematite bands. Oxidizing conditions of formation were also argued for mineral assemblages containing the dehydrogenated end-member amphibole ungarettiite, $NaNa_2(Mn_2^{2+}Mn_3^{3+})Si_8O_{22}O_2$ (Hawthorne et al. 1995). The latter crystallized, like balestraite, during low-*T* metamorphic recrystallization of submarine Mn-rich deposits at the Hoskins mine (Grenfell, New South Wales, Australia). A further linking between the formation of balestraite and ungarettiite, besides the concomitant occurrence of calcite and quartz bands, is represented by their common Mn- and Li-rich

mineral assemblage characterized by the presence of braunite, norrishite, and sugilite. As a whole, such a match suggests that both the composition of the manganese deposit and its hydrothermal alteration were similar in the Hoskin and Cerchiara occurrences.

Balestraite and ungarettiite may be assumed to form where host rocks enriched in transition elements reacted with alkaline fluids at low-*T* conditions, thus producing unusual alkali-rich amphiboles and micas completely dehydrogenated and containing highly oxidized transition elements (Mn and V). Further investigations are needed to determine whether the strongly oxidizing conditions controlling the crystallization of balestraite and ungarettiite were the result of a buffering effect exerted by the transition-element-rich host matrix or a primary feature of the flowing fluids, the latter possibly CO_2 rich.

IMPLICATIONS

Vanadium in minerals may be present in variable oxidation states forming polyhedra with different coordination number [e.g. tetrahedral (V^{5+}), trigonal bipyramidal (V^{4+}, V^{5+}) and octahedral (mainly V^{3+} and, to lesser extent, V^{4+} and V^{5+})], and therefore its presence in complex solid solutions adds difficulties in the determination of cation distribution. For the V-members of the mica group, i.e. chernykhite (Ankinovich et al. 1973) and roscoelite (Brigatti et al. 2003), vanadium is nominally present as V^{3+} (i.r. = 0.64 Å, Shannon 1976). However, variable amounts of V^{4+} and V^{5+} cations, which are similar in radii size (0.58 and 0.54 Å, respectively) may coexist in octahedral sites. According to Ankinovich et al. (1973), in the Ba-bearing muscovites and chernykhite from the Karatau carbonaceous-siliceous schists, micas hosted in rocks enriched in organic matter contain V^{3+}, whereas V^{4+} occurs in micas from rocks poor in organic matter and may sometimes replace V^{3+}. Balestraite, a near V^{5+} end-member, allows the evaluation of the structural effect of V^{5+} within the octahedral sheet in micas.

Moreover, balestraite enlarges the number of dehydrogenated rock forming minerals (amphiboles and micas) containing highly oxidized transition elements. The incorporation in the mica structure of V^{5+} allows for a mechanism to charge balance the incorporation ‘oxy’ component in micas.

ACKNOWLEDGMENTS

The manuscript benefited from the revisions of Stephen J. Guggenheim and an anonymous reviewer and from demanding and perceptive comments of the members of the IMA-CNMNC. Thanks are due also to Fabrizio Castellaro for providing the sample and Roberto Bracco for the photo of balestraite. Francesco Di Benedetto is thanked for the acquisition of the EPR spectrum. X-ray intensity data were collected at CRIST, Centro di Cristallografia Strutturale, University of Florence, Italy.

REFERENCES CITED

Ankinovich, S.G., Ankinovich, Ye.A., Rozdestvenskaya, I.V., and Frank-Kamenetsky, V.A. (1973) Chernykhite, a new barium-vanadium mica from northwestern Karatau. International Geology Review, 15, 641-647.

Ankinovich, E.A., Bekenova, G.K., Kompaneitsev, V.P., Kotelnikov, P.E., and Savostin, B.A. (2001) Vanadium and vanadium-bearing micas from the carbonaceous-siliceous formation of the Bolshoi Karatau Ridge (South Kazakhstan). 2. V^{4+}-Ba phengite. Vanadium-bearing muscovite and phengite. Geologia Kazakhstana, 2, 13-23 (in Russian).

Baumgartner, A., Butterhof, C., Koch, S., Mariychuk, R., and Breu, J. (2009) Melt synthesis and characterization of synthetic Mn-rich tainiolite. Clays and Clay Minerals, 57, 271-277.

Baur, W. H. (1978) Variation of mean Si-O bond lengths in silicon-oxygen tetrahedra. Acta Crystallographica, B34, 1751-1756.

Brese, N.E., and O'Keeffe, M. (1991) Bond-valence parameters for solids. Acta Crystallographica, B47, 192-197.

Brigatti, M.F., Caprilli, E., Marchesini, M., and Poppi, L., (2003) The crystal structure of roscoelite-1*M*. Clays and Clay Minerals, 51, 301-308.

Brigatti, M.F., and Guggenheim, S. (2002) Mica crystal chemistry and the influence of pressure, temperature, and solid solution on atomistic models. In A. Mottana, F.P. Sassi, J.B. Thompson Jr., and S. Guggenheim, Eds., Micas: crystal chemistry and metamorphic petrology. Reviews in Mineralogy and Geochemistry, 46, 1-97.

Brigatti, M.F., Lugli, C., Poppi, L., Foord, E.E., and Kile, D.E. (2000) Crystal chemical variations in Li- and Fe-rich micas from the Pikes Peak batholith (central Colorado). American Mineralogist, 85, 1275-1286.

Brigatti, M.F., Mottana, A., Malferrari, D., and Cibin, G. (2007) Crystal structure and chemical composition of Li-, Fe-, and Mn-rich micas. American Mineralogist, 92, 1395-1400.

Burns, D.T., and Flockhart, B.D. (1990) Application of Quantitative EPR [and Discussion]. Philosophical Transactions of the Royal Society of London A, 333(1628), 37- 48.

Cabella, R., Lucchetti, G., and Marescotti, P. (1998) Mn-ores from Eastern Ligurian ophioltic sequences ("Diaspri di Monte Aple" Formation, Northern Apennines, Italy). Trends in Mineralogy, 2, 1-17.

Cabella, R., Lucchetti, G., and Palenzona A. (1990) Al-rich, Fe-poor manganoan sugilite in a pectolite-bearing assemblage from Cerchiara Mine (Northern Appennines, Italy). Neues Jahrbuch für Mineralogie Monatshefte, 1990, 443-448.

Canil, D. (2002) Vanadium in peridotites, mantle redox and tectonic environments: Archean to present. Earth and Planetary Science Letters, 195, 75-90.

Cesare, B., Cruciani, G., and Russo, U. (2003) Hydrogen deficiency in Ti-rich biotite from anatectic metapelites (El Joyazo, SE Spain): Crystal-chemical aspects and implications for high-temperature petrogenesis. American Mineralogist, 88, 583–595.

Chukanov, N.V., Mukhanova, A.A., Rastsvetaeva, R.K., Belakovsky, D.I., Möckel, S., Karimova, O.V., Britvin, S.N., and Krivovichev, S.V. (2011) Oxyphlogopite $K(Mg,Ti,Fe)_3[(Si,Al)_4O_{10}](O,F)_2$: A new mineral species of the mica group. Geology of Ore Deposits, 53, 583-590.

Cortesogno, L., Lucchetti, G., and Penco, A.M. (1979) Le mineralizzazioni a manganese nei diaspri delle ofioliti liguri: mineralogia e genesi. Rendiconti della Società Italiana di Mineralogia e Petrologia, 35, 151-197.

Cruciani, G., and Zanazzi, P.F. (1994) Cation partitioning and substitution mechanisms in 1*M* phlogopite; a crystal chemical study. American Mineralogist, 79, 289-301.

Frost, R.L., Erickson, K.L., Weier, M.L., and Carmody, O. (2005) Raman and infrared spectroscopy of selected vanadates. Spectrochimica Acta, Part A: Molecular and

391 Biomolecular Spectroscopy, 61, 829-834.
392 Gianfagna, A., Scordari, F., Mazziotti Tagliani, S., Ventruti G., and Ottolini, L. (2007)
393 Fluorophlogopite from Biancavilla (Mt. Etna, Sicily, Italy): Crystal structure and
394 crystal chemistry of a new F-dominant analog of phlogopite. American Mineralogist,
395 92, 1601-1609.
396 Giuliani, G., Ohnenstetter, D., Palhol, F., Feneyrol, J., Boutroy, E., De Boissezon, H. and
397 Lhomme, T. (2008) Karelianite and vanadian phlogopite from the Merelani Hills gem
398 zoisite deposits, Tanzania. Canadian Mineralogist, 46, 1183-1194.
399 Güven, N. (1971) The crystal structure of $2M_1$ phengite and $2M_1$ muscovite. Zeitschrift für
400 Kristallographie, 134, 195-212.
401 Hawthorne, F.C., Oberti, R., Cannillo, E., Sardone, N., Zanetti, A., Grice, J.D., and Ashley,
402 P.M. (1995) A new anhydrous amphibole from Hoskins mine, Grenfell, New South
403 Wales, Australia: Description and crystal structure of ungarettiite,
404 $NaNa_2(Mn_2^{2+}Mn_3^{3+})Si_8O_{22}O_2$. American Mineralogist, 80, 165-172.
405 Hazen, R.M., and Burnham, C.W. (1973) The crystal structure of one layer phlogopite and
406 annite. American Mineralogist, 58, 889-900.
407 Koch, S., and Breu, J. (2013) Transition metals in micas: synthesis and characterization of
408 Co-rich Cs-tainiolite. European Journal of Mineralogy, 25, 487-494.
409 Kogarko, L.N., Uvarova, Yu.A., Sokolova, E., Hawthorne, F.C., Ottolini, L., and Grice J.D.
410 (2005) Oxykinoshitalite, a new species of mica from Fernando de Noronha Island,
411 Pernambuco, Brazil; occurrence and crystal structure. Canadian Mineralogist, 43,
412 1501-1510.
413 Kunz, M., Armbruster, T., Lager, G.A., Schultz, A.J., Goyette, R.J., Lottermoser, W., and
414 Amthauer, G. (1991) Fe,Ti ordering and octahedral distortions in acentric neptunite:
415 Temperature dependent X-ray and neutron structure refinements and Mössbauer
416 spectroscopy. Physics and Chemistry of Minerals, 18, 199-213.
417 Laurora, A., Brigatti, M.F., Mottana, A., Malferrari, D., and Caprilli, E. (2007) Crystal
418 chemistry of trioctahedral micas in alkaline and subalkaline volcanic rocks: A case
419 study from Mt. Sassetto (Tolfa district, Latium, central Italy). American Mineralogist,
420 92, 468-480.

Lucchetti, G., Cortesogno, L., and Palenzona, A. (1988) Low-temperature metamorphic mineral assemblages in Mn-Fe ores from Cerchiara mine (northern Appennine, Italy). Neues Jahrbuch für Mineralogie Monatshefte, 1988, 367-383.

Mariychuk, R., Baumgartner, A., Wagner, F.E., Lerf, A., Dubbe, A., and Breu, J. (2007) Synthesis, structure and electric conductivity of ferrous tainiolite and its oxidative conversion into coarse-grained swellable smectite. Chemistry of materials, 19, 5377-5387.

Matarrese, S., Schingaro, E., Scordari, F., Stoppa, F., Rosatelli, G., Pedrazzi, G., and Ottolini, L. (2008) Crystal chemistry of phlogopite from Vulture-S. Michele Subsynthem volcanic rocks (Mt. Vulture, Italy) and volcanological implications. American Mineralogist, 93, 426-437.

Mesto, E., Schingaro, E., Scordari, F., and Ottolini, L. (2006) An electron microprobe analysis, secondary ion mass spectrometry, and single-crystal X-ray diffraction study of phlogopites from Mt. Vulture, Potenza, Italy: Consideration of cation partitioning. American Mineralogist, 91, 182-190.

Miller, C., Zanetti, A., Thöni, M., and Konzett, J. (2007) Trace element mineral chemistry of the type locality (Koralpe, Saualpe) and Pohorje eclogites (Eastern Alps): implications for behaviour of fluid-mobile elements in a continental subduction zone, geochronology and geothermometry. Chemical Geology, 239, 96-123.

Ohta, T., Takeda, H., and Takeuchi, Y. (1982) Mica Polytypism: Similarities in the Crystal Structures of Coexisting 1*M* and 2*M* Oxybiotites. American Mineralogist, 67, 298-310.

Oxford Diffraction (2006) *CrysAlis* RED (Version 1.171.31.2) and ABSPACK in *CrysAlis*RED. Oxford Diffraction Ltd, Abingdon, Oxfordshire, England.

Pan, Y., and Fleet, M. E. (1992) Mineral chemistry and geochemistry of vanadian silicates in the Hemlo gold deposit, Ontario, Canada. Contributions to Mineralogy and Petrology, 109, 511-525.

Parsons, S., and Flack, H. (2004) Precise absolute-structure determination in light-atom crystals. Acta Crystallographica, A60, s61.

Robinson, K., Gibbs, G.V., and Ribbe, P.H. (1971) Quadratic elongation: A quantitative measure of distortion in coordination polyhedra. Science, 172, 567–570.

Schindler, M., Hawthorne, F.C., and Baur, W.H. (2000) Crystal chemical aspects of vanadium: polyhedral geometries, characteristic bond valences, and polymerization of (VO_n) polyhedral. Chemistry of Materials, 12, 1248-1259.

Schingaro, E., Lacalamita, M., Scordari, F., Brigatti, M.F., and Pedrazzi, G. (2011) Crystal chemistry of Ti-rich fluorophlogopite from Presidente Olegario, Alto Paranaíba igneous province, Brazil. American Mineralogist, 96, 732-743.

Scordari, F., Dyar, M.D., Schingaro, E., Lacalamita, M., and Ottolini, L. (2010) XRD, micro-XANES, EMPA, and SIMS investigation on phlogopite single crystals from Mt. Vulture (Italy). American Mineralogist, 95, 1657-1670.

Scordari, F., Schingaro, E., Ventruti, G., Lacalamita, M., and Ottolini, L. (2008) Red micas from basal ignimbrites of Mt. Vulture (Italy): interlayer content appraisal by a multi-methodic approach. Physics and Chemistry of Minerals, 35, 163-174.

Scordari, F., Schingaro, E., Ventruti, G., Nicotra, E., Viccaro, M., and Mazziotti Tagliani, S. (2013) Fluorophlogopite from Piano delle Concazze (Mt. Etna, Italy): Crystal chemistry and implications for the crystallization conditions. American Mineralogist, 98, 1017-1025.

Shannon, R.D. (1976) Revised effective ionic radii and systematic studies of interatomic distances in halides and chalcogenides. Acta Crystallographica, A32, 751-767.

Sheldrick, G.M. (2008) A short history of SHELX. Acta Crystallographica, A64, 112-122.

Takeda, H., and Burnham, C.W. (1969) Fluor-polylithionite: a lithium mica with nearly hexagonal $(Si_2O_5)^{2-}$ ring. Mineralogical Journal, 6, 102-109.

Tiepolo, M., Zanetti, A., and Vannucci, R. (2005) Determination of Li, Be and B at trace levels by LA-ICP-MS. Geostandards and Geoanalytical Research, 29, 211-224.

Toraya, H., Iwai, S., Marumo, F., and Hirao, M. (1977) The crystal structure of taeniolite, $KLiMg_2Si_4O_{10}F_2$. Zeitschrift für Kristallographie, 146, 73-83.

Tyrna, P.L., and Guggenheim, S. (1991) The crystal structure of norrishite, $KLiMn^{3+}{}_2Si_4O_{12}$: an oxygen-rich mica. American Mineralogist, 76, 266-271.

Wilson, A.J.C., and Prince, E., Eds. (1999) *International Tables for X-ray Crystallography*,

Volume C: Mathematical, physical and chemical tables (2nd Edition), KluwerAcademic, Dordrecht, NL.

Zanetti, A., Tiepolo, M., Oberti, R., and Vannucci, R. (2004) Trace-element partitioning in olivine: modelling of a complete data set from a synthetic hydrous basanite melt. Lithos, 75, 39-54.

CAPTION OF FIGURES

Figure 1. Balestraite from Cerchiara mine associated with quartz and calcite (R. Bracco photo); field of view is 2 mm.

Figure 2. The octahedral sheet of balestraite viewed down the *c* axis. M1 and M3 octahedra host Li^{+}, V^{5+} occupies M2.

Figure 3. Raman spectrum of balestraite.

Figure 4. [2+2+2]-coordination of V^{5+} in the M2 octahedron.

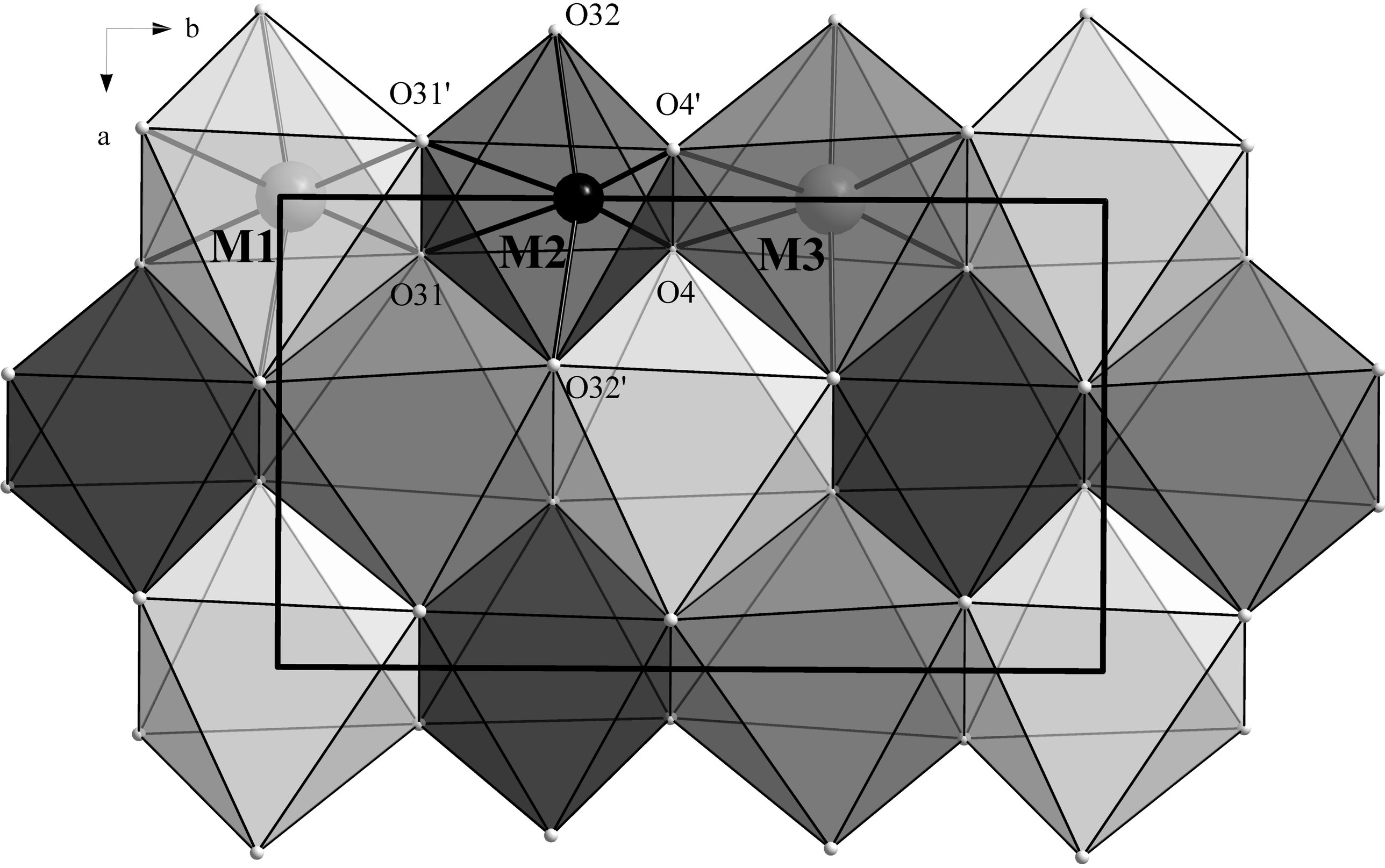
b
a
O32
O31'
O4'
M1
M2
M3
O31
O4
O32'

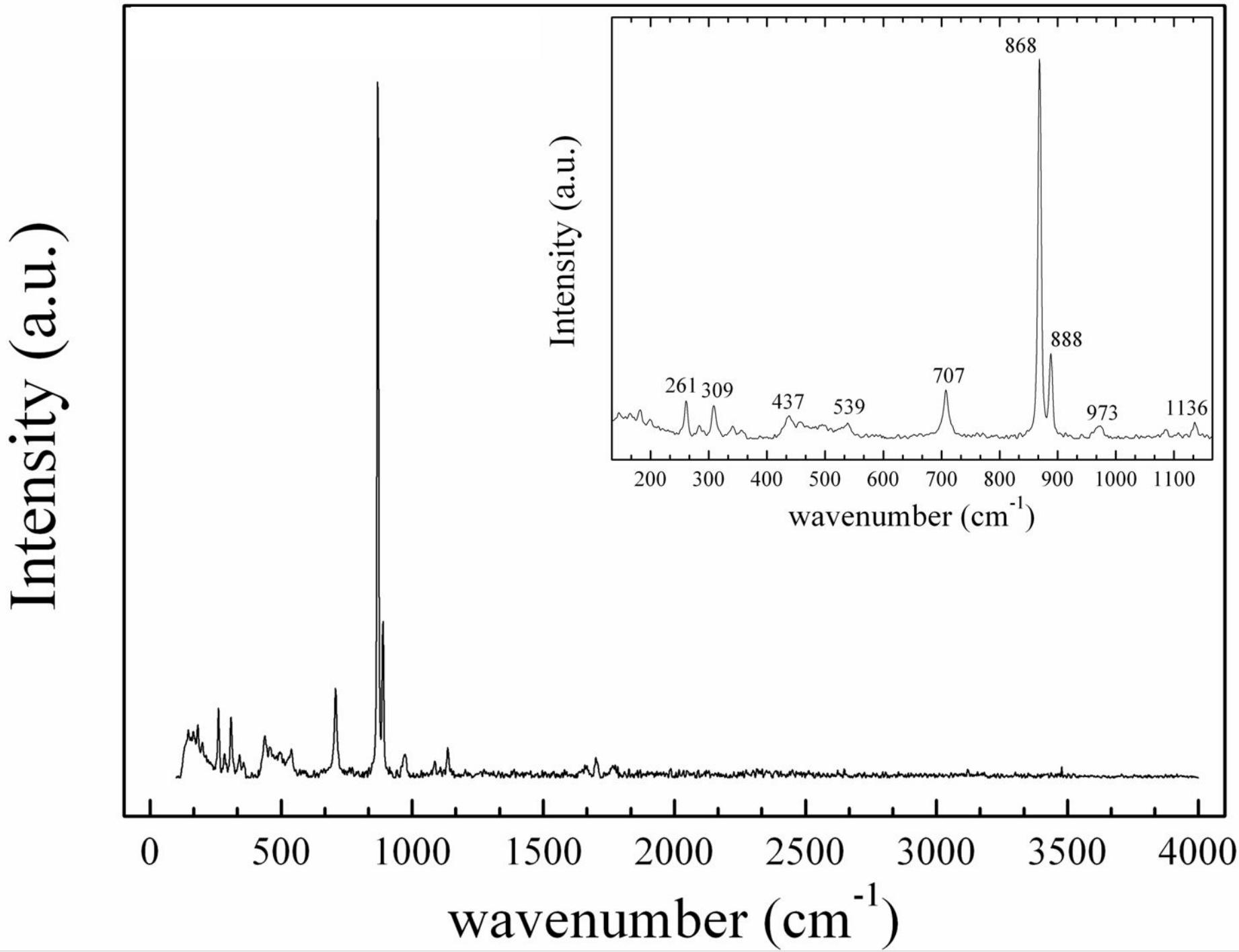
Intensity (a.u.)
0
500
1000
1500
2000
2500
3000
3500
4000
wavenumber (cm-1)
Intensity (a.u.)
868
888
261
309
437
539
707
973
1136
200
300
400
500
600
700
800
900
1000
1100
wavenumber (cm-1)

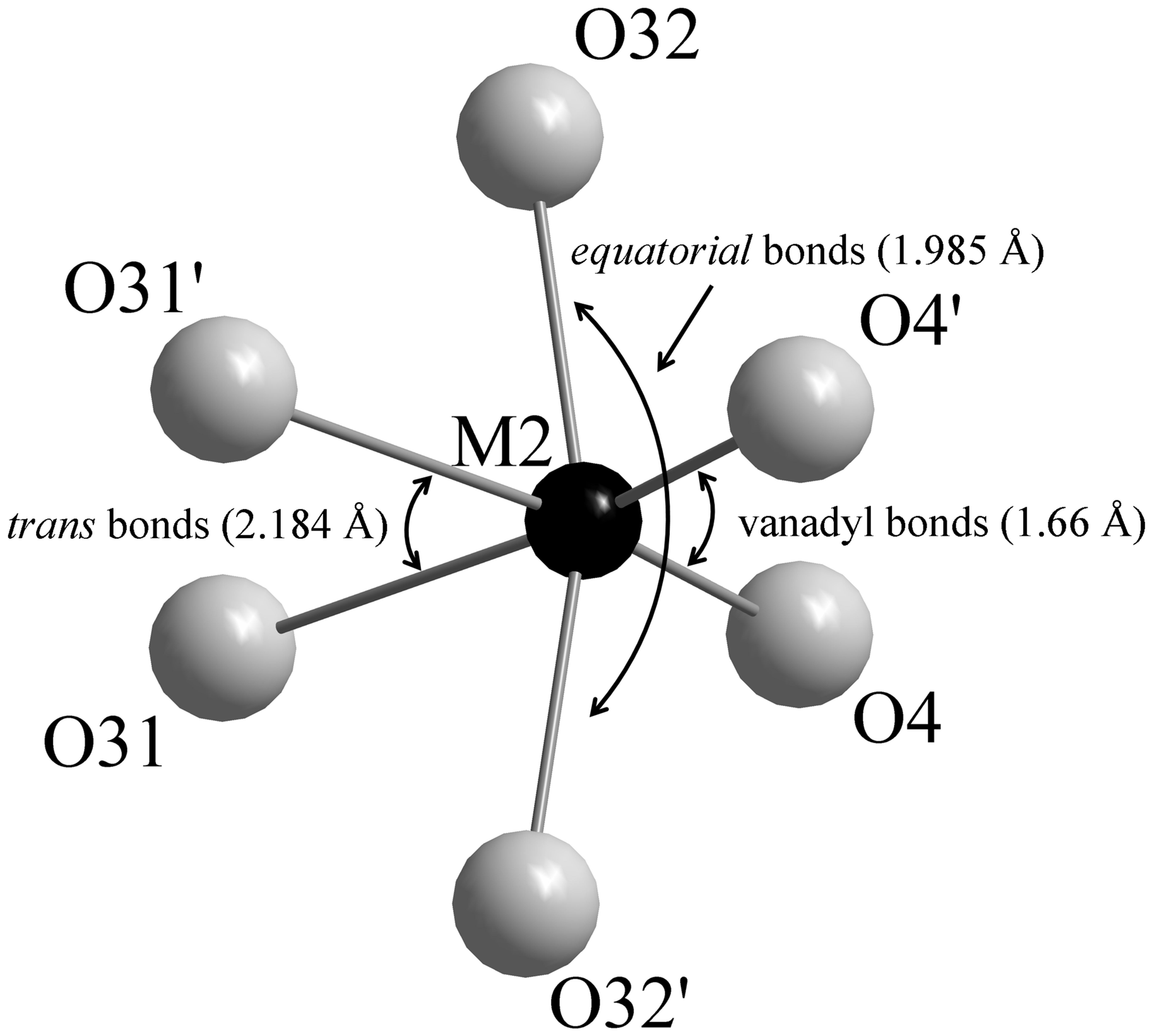
O32
O31'
equatorial bonds (1.985 Å)
O4'
M2
trans bonds (2.184 Å)
vanadyl bonds (1.66 Å)
O31
O4
O32'

Table 1 – Crystallographic data and refinement parameters for balestraite

Crystal data	
Ideal formula	$KLi_2V^{5+}Si_4O_{12}$
Crystal system	monoclinic
Space group	*C*2
Unit-cell parameters (Å, °)	5.2024(5) 8.9782(7) 9.997(2) 100.40(2)
Unit-cell volume (Å^3)	459.3(1)
Z	2
Crystal size (mm)	0.030 × 0.220 × 0.250
Data collection	
Diffractometer	Oxford Diffraction Xcalibur 3
Temperature (K)	293(3)
Radiation, wavelength (Å)	Mo*K*α, 0.71073
2θ max for data collection (º)	63.98
Crystal-detector dist. (mm)	50
h, *k*, *l* ranges	-7 to 7, -13 to 13, -14 to 14
Axis, frames, width (º), time per frame (s)	ω, 515, 1.00, 10
Total reflections collected	14541
Unique reflections	1587
Unique reflections $I > 3\sigma(I)$	1302
Data completeness to θ_{max} (%)	98.3
Absorption correction method	ABSPACK (Oxford Diffraction 2006)
Structure refinement	
Refinement method	Full-matrix least-squares on F^2
Data/restraints/parameters	1587/1/60
R_1 [$F_o > 2\sigma(F_o)$], wR_2 [$F_o > 2\sigma(F_o)$]	0.127, 0.342
R_1 all, wR_2 all	0.138, 0.345
Goodness-of-fit on F^2	1.025
Largest diff. peak and hole (e$^-$/Å^3)	1.09, -1.48

$$R_{int} = (n/n-1)^{1/2}\left[F_o^2 - F_o(mean)^2\right]/\sum F_o^2$$

$$R_1 = \sum||F_o| - |F_c||/\sum|F_o| \qquad wR_2 = \left\{\sum\left[w\left(F_o^2 - F_c^2\right)^2\right]/\sum\left[w\left(F_o^2\right)^2\right]\right\}^{1/2}$$

$$GooF = \left\{\sum\left[w\left(F_o^2 - F_c^2\right)^2\right]/(n-p)\right\}^{1/2}$$ where n = no. of reflections, p = no. of refined parameters

Table 2 – Atoms, site occupancy factors (s.o.f.), fractional atom coordinates, and equivalent isotropic displacement parameters (Å^2) for balestraite.

Atom	s.o.f.	*x/a*	*y/b*	*z/c*	U_{iso}
K	$K_{1.00}$	0	0.5021(5)	0	0.043(1)
M1	$Li_{1.00}$	0	0.012(3)	½	0.019(4)
M2	$V_{0.93(2)}Li_{0.07}$	0	0.3612(3)	½	0.031(1)
M3	$Li_{0.97(2)}V_{0.03}$	0	0.681(2)	½	0.018(8)
T1	$Si_{1.00}$	0.0766(6)	0.1706(3)	0.2320(4)	0.030(1)
T2	$Si_{1.00}$	0.5820(6)	0.3354(3)	0.2290(3)	0.029(1)
O1	$O_{1.00}$	0.056(2)	0.003(1)	0.1682(8)	0.032(2)
O21	$O_{1.00}$	0.307(2)	0.2535(9)	0.1689(9)	0.029(2)
O22	$O_{1.00}$	0.806(2)	0.2524(9)	0.1601(9)	0.031(2)
O31	$O_{1.00}$	0.123(2)	0.1712(9)	0.3906(8)	0.024(2)
O32	$O_{1.00}$	0.646(2)	0.332(1)	0.3902(8)	0.030(2)
O4	$O_{1.00}$	0.106(2)	0.474(1)	0.3901(9)	0.041(2)

Table 3 – Anisotropic displacement parameters of the atoms for balestraite.

Atom	U_{11}	U_{22}	U_{33}	U_{23}	U_{13}	U_{12}
K	0.036(2)	0.025(2)	0.069(3)	0	0.012(2)	0
M2	0.017(1)	0.011(1)	0.067(3)	0	0.012(1)	0
T1	0.018(2)	0.014(1)	0.058(3)	0.001(1)	0.010(1)	−0.001(1)
T2	0.019(2)	0.017(2)	0.050(2)	0.001(1)	0.009(1)	0.001(1)

Note: M1, M3 and the oxygen atoms refined as isotropic.

Table 5 – Observed and calculated X-ray powder diffraction data for balestraite.

			(a)		(b)	
h	*k*	*l*	*d*(Å)	I_{obs}/I_{100}	*d*(Å)	I_{calc}/I_{100}
0	0	1	9.9	50	9.8328	41
0	0	2	4.96	20	4.9164	14
0	2	0	4.51	100	4.4891	40
1	1	0			4.4456	22
-1	1	1	4.34	40	4.3127	49
0	2	1	4.11	25	4.0836	29
1	1	1	3.85	10	3.8315	17
-1	1	2	3.60	40	3.5893	100
0	2	2	3.34	30	3.3151	66
0	0	3	3.30	30	3.2776	32
1	1	2	3.08	35	3.0668	93
-1	1	3	2.877	10	2.8611	26
0	2	3	2.662	15	2.6471	29
-2	0	1	2.592	70	2.5927	15
1	3	0			2.5833	39
2	0	0	2.574	70	2.5585	23
-1	3	1			2.5565	38
1	1	3			2.4602	4
0	0	4	2.460	10	2.4582	4
1	3	1			2.4444	8
-1	3	2	2.385	70	2.3778	39
2	0	1			2.3738	25
-1	1	4	-	-	2.3101	7
-2	2	1	2.251	10	2.2451	9
2	2	0	2.232	10	2.2228	12
0	4	1	2.198	20	2.1883	22
-2	2	2	2.167	10	2.1563	10
-1	3	3	2.133	15	2.1252	18
2	0	2	2.13	s	2.1183	11
2	2	1	2.10	s	2.0985	8
0	0	5	1.976	25	1.9666	15
-2	0	4	-	-	1.9579	5
1	3	3	1.957	10	1.9446	12
-2	2	4	1.817	5	1.7947	4
-3	1	1	1.703	<5	1.7026	4
0	4	4	1.657	<5	1.6575	6
1	5	1			1.6533	4
-1	3	5	1.642	15	1.6384	26
2	0	4	1.63	s	1.6315	12
2	4	1			1.6309	8
-3	1	3	1.614	5	1.6124	4
-2	4	3	1.583	5	1.5786	11
1	5	2			1.5732	4

-1	5	3	1.546	5	1.5432	6
-3	1	4	1.512	<5	1.5153	4
-2	0	6			1.5093	5
3	1	2			1.5066	6
-3	3	1	1.503	50	1.5004	23
1	3	5			1.5002	8
0	6	0	1.486	5	1.4964	10
2	2	5	-	-	1.3701	5
-2	0	7	1.338	5	1.3374	6
1	3	6			1.3301	12
-4	0	1	-	-	1.2989	4
-4	0	2	-	-	1.2964	4
-2	6	1	1.299	10	1.2960	10
2	6	0			1.2917	7
-3	3	5	1.284	5	1.2842	4

(a) = observed diffraction pattern obtained by converting the diffraction rings into a conventional XRD pattern; (b) = calculated diffraction pattern obtained from structural data (only reflections with $I_{calc}/I_{100} \geq 4$ are listed); s = shoulder of a peak.

Table 6 – Electron microprobe analyses (means and ranges in wt% of oxides) and atomic ratios (on the basis of 12 oxygen atoms) of balestraite

	mean	range	atom	atomic ratios
K_2O	11.24	11.19 – 11.28	K	0.99
Li_2O*	7.20	7.04 – 7.46	Li	2.00
V_2O_5	21.15	21.03 – 21.28	V	0.97
SiO_2	58.46	58.06 – 58.76	Si	4.04
total	98.05		$\Sigma_{cations}$	8.00

Note: * Li determined by LA-ICP-MS (three point analyses on different spots); Mn_2O_3 up to 0.12 wt% corresponding to 0.006 atoms per formula units.

Table 7 – Bond distances (Å) for balestraite

M1		**M2**		**M3**	
O31$^{i, ii}$	1.97(2)	O4$^{i, ii}$	1.66(1)	O32$^{v, vi}$	1.98(2)
O32$^{iii, iv}$	2.17(2)	O32$^{vii, xiii}$	1.985(9)	O31$^{v, vi}$	2.067(8)
O4$^{iii, iv}$	2.17(1)	O31$^{i, ii}$	2.184(8)	O4$^{i, ii}$	2.27(2)
mean	2.10	*mean*	1.943	*mean*	2.10
T1		**T2**		**K**	
O31^{i}	1.560(8)	O32^{i}	1.586(9)	O22$^{viii, xiv}$	3.031(9)
O22^{vii}	1.63(1)	O1^{xii}	1.620(9)	O22$^{vi, ix}$	3.038(9)
O1^{i}	1.63(1)	O21^{i}	1.624(9)	O21$^{i, x}$	3.068(9)
O21^{i}	1.632(9)	O22^{i}	1.637(9)	O1$^{ii, xi}$	3.074(8)
mean	1.613	*mean*	1.617	O21$^{ix, xv}$	3.092(9)
				O1$^{ix, xv}$	3.092(8)
				mean	3.066

Symmetry codes: (*i*) *x*, *y*, *z*; (*ii*) −*x*, *y*, −*z*+1; (*iii*) *x*−½, *y*−½, *z*; (*iv*) −*x*+½, *y*−½, −*z*+1; (*v*) −*x*+½, *y*+½, −*z*+1; (*vi*) *x*−½, *y*+½, *z*; (*vii*) *x*−1,*y*, *z*; (*viii*) −*x*+1, *y*, −*z*; (*ix*) −*x*+½, *y*+½, −*z*; (*x*) −*x*, *y*, −*z*; (*xi*) −*x*−½, *y*+½, −*z*; (*xii*) *x*+½, *y*+½, *z*; (*xiii*) −*x*+1, *y*, −*z*+1; (*xiv*) *x*+1, *y*, *z*; (*xv*) *x*+½, *y*-½, *z*.

Table 8 – Selected structural parameters for balestraite

Whole layer		**Oct. sheet**	
Δ_{TM} (Å)	0.298	V_{M1} (Å^3)	12.03
β_{ideal}	99.989	V_{M2} (Å^3)	9.54
intralayer shift	-0.347*a*	V_{M3} (Å^3)	12.10
		ψ_{M1} (°)	59.147
Interlayer		ψ_{M2} (°)	56.279
V (KO_{12}) (Å^3)	57.76	ψ_{M3} (°)	59.185
t_{int} (Å)	3.259	OAV_{M1}	70.90
<K-O>$_{inner}$ (Å)	3.066	OAV_{M2}	58.76
<K-O>$_{outer}$ (Å)	3.066	OAV_{M3}	71.22
		OQE_{M1}	1.0229
Tet. sheet		OQE_{M2}	1.0295
α (°)	0.15	OQE_{M3}	1.0251
Δ*z* (Å)	0.087	BLD_{M1}	4.227
τ_{T1} (°)	113.54	BLD_{M2}	9.712
τ_{T2} (°)	112.50	BLD_{M3}	5.204
TAV_{T1}	21.62	ELD_{M1}	5.187
TAV_{T2}	11.66	ELD_{M2}	1.671
TQE_{T1}	1.0047	ELD_{M3}	5.238
TQE_{T2}	1.0026	$Shift_{M2}$(Å)	+0.316
BLD_{T1}	1.643	$Shift_{M3}$(Å)	-0.198
BLD_{T2}	0.951	$t_{M(O3)}$ (Å)	2.155
V_{T1} (Å^3)	2.14	$t_{M(O4)}$ (Å)	2.161
V_{T2} (Å^3)	2.16	$t_{M(O3\text{-}O4)}$ (Å)	2.157
t_{tet} (Å)	2.221		

Notes: t_{tet} = tetrahedral sheet thickness calculated from *z* coordinates of basal and apical O atoms; TQE = tetrahedral quadratic elongation (Robinson et al. 1971); TAV = tetrahedral angle variance (Robinson et al. 1971); τ = tetrahedral flattening angle; α = tetrahedral rotation angle (Hazen and Burnham 1973); Δ*z* = departure from co-planarity of the basal O atoms (Güven 1971); Δ_{TM} = $2\sqrt{3}$<O-O>$_{basal}$-$3\sqrt{2}$(<M1-O>+<M2-O>+<M3-O>)/3; ψ = octahedral flattening angles (Hazen and Burnham 1973); BLD and ELD = octahedral bond-length and edge-length distortion parameters (Kunz et al. 1991); $Shift_{M2,3}$ = off-center shift (Laurora et al. 2007) "+" and "-" related respectively to a migration towards or away from (010) plane; OQE = octahedral quadratic elongation (Robinson et al. 1971); OAV = octahedral angle variance (Robinson et al. 1971); $t_{M(O3\text{-}O4)}$, $t_{M(O3)}$, $t_{M(O4)}$, octahedral sheet thickness calculated from the *z* coordinates, respectively, of all oxygens bonded to octahedral cations (O3 and O4), of only the tetrahedral apical oxygens (O3), and of only oxygens bonded to hydrogens (O4) (Toraya 1981); t_{int} calculated

from the *z* coordinates of basal O atoms; $\langle K\text{-}O \rangle_{inner/outer}$ = mean bond length for *inner*/*outer* K-O bonds: K-O22^{viii,xiv}, -O1^{ii,xi}, -O21^{ix,xv} and K-O21^{ix,xv}, -O22^{vi,ix}, -O1^{ix,xv}, respectively.

Table 9 – Bond-valence (*v.u.*) arrangement for balestraite

	K	M1 (Li)	M2 (V^{5+})	M3 (Li)	T1	T2	Σ O
O1	$0.078^{\times 2\downarrow}/0.075^{\times 2\downarrow}$				1.027	1.056	2.24
O21	$0.080^{\times 2\downarrow}/0.075^{\times 2\downarrow}$				1.022	1.044	2.22
O22	$0.086^{\times 2\downarrow}/0.088^{\times 2\downarrow}$				1.016	1.008	2.20
O31		$0.256^{\times 2\downarrow}$	$0.357^{\times 2\downarrow}$	$0.197^{\times 2\downarrow}$	1.241		2.05
O32		$0.149^{\times 2\downarrow}$	$0.611^{\times 2\downarrow}$	$0.248^{\times 2\downarrow}$		1.157	2.17
O4		$0.148^{\times 2\downarrow}$	$1.476^{\times 2\downarrow}$	$0.114^{\times 2\downarrow}$			1.74
	0.96	1.11	4.89	1.12	4.31	4.27	

Note: calculated from the bond-valence curves of Brese and O'Keeffe (1991) assuming the ideal formula $KLi_2V^{5+}Si_4O_{10}O_2$.